Int. J. Electrochem. Sci., 15 **(2020)** 3382 – 3399, doi: 10.20964/2020.04.49

International Journal of
ELECTROCHEMICAL
SCIENCE
www.electrochemsci.org

Electrochemical oxidation of Hydrolyzed Polyacrylamide (HPAM) at Ti/SnO_2-Sb_2O_3/β-PbO_2 Anode. Degradation Kinetics and Mechanisms

Yanhe Han[1,2*], *Sitao Zhang*[1,2,3], *Xiaofei Zhang*[1], *Jiaqing Chen*[2*]

[1] State Key Laboratory of Petroleum Pollution Control, CNPC Research Institute of Safety and Environmental Technology, Beijing 100007, China
[2] Department of Environmental Engineering, Beijing Institute of Petrochemical Technology, Beijing 102617, China
[3] Beijing University of Technology, Beijing 100124, China
[*]E-mail: hanyanhe@bipt.edu.cn, jiaqing@bipt.edu.cn

Received: 23 December 2019 / *Accepted:* 10 February 2020 / *Published:* 10 March 2020

Polymer flooding produced water is a taxonomic group of refractory wastewaters with a high viscosity and molecular weight. The discharge of water that contains hydrolyzed polyacrylamide (HPAM) into the environment will result in many environmental problems. The use of the electro-oxidation (EO) method for the degradation of wastewater is characterized by many advantages, including high efficiency, wide applicability, simplicity, and easy operation. In this study, HPAM was degraded using Ti/SnO_2+Sb_2O_3/β-PbO_2 anodes. The physicochemical properties of the electrodes were characterized via scanning electron microscopy (SEM) and X-ray diffraction (XRD). HPAM degradation experiments were carried out at current densities of 10-40 mA/cm^2, electrode distances of 1-5 cm, initial solution pH values of 3-7, and electrolyte concentrations of 2000-10000 mg/L. The degradation kinetics studies showed that the HPAM degraded by the EO process followed a pseudo-first-order kinetic model under various conditions. Under the optimal conditions, namely a current density of 20 mA/cm^2, electrode distance of 1 cm, initial pH of 5, and electrolyte concentration of 6000 mg/L, the efficiency of the electrochemical degradation of HPAM attained 100%. Finally, the degradation mechanism and products of HPAM were determined via monitoring ion chromatography (IC), three-dimensional excitation emission matrix (3D EEM) fluorescence spectra, Fourier transform infrared spectroscopy (FT-IR), the total organic carbon (TOC), and gas chromatography/mass spectrometry (GC/MS).

Keywords: Electro-oxidation, HPAM, kinetics, mechanism.

1. INTRODUCTION

Hydrolyzed polyacrylamide (HPAM) has been widely used in oil production processes, as it can reduce water mobility, neutralize charges, and agglomerate particles, thereby effectively increasing the

rate of oil exploitation. However, a large amount of polyacrylamide wastewater is produced during oil recovery, and although most is recycled, the rest is released into the environment [1]. The wastewater has the characteristics of a high viscosity, high COD, and serious emulsification, and is also characterized by biological toxicity. As a linear polymer compound of acrylamide monomers, substandard discharge into the environment is likely to cause equipment corrosion, scaling, a blocking layer, and the contamination of underground water. Furthermore, the residual HPAM that is broken down into acrylamide monomers is harmful to human health and ecological environments [2]. Therefore, it must be treated before reinjection and discharge.

The reported treatments of HPAM wastewater include physical [3, 4], chemical [5, 6], and biological [7, 8] treatments, but these methods have many disadvantages that coincide with the degradation of HPAM. The chemical precipitation method has been found to be efficient for the treatment of HPAM wastewater, but it requires the use of expensive drugs and is costly. The biodegradation method has the disadvantages of a long treatment cycle, large reaction equipment, and difficulty in screening and cultivating strains. Compared with the traditional methods, electrochemistry techniques have gained significant popularity in recent years for the treatment of refractory wastewater, such as wastewater from the pharmaceutical [9], textile [10], and petrochemical [11] industries. The experimental conditions of the electrocoagulation degradation of HPAM were optimized, and it was found that while $Al(OH)_3$ floc and active chlorine are helpful for HPAM degradation, they cause secondary pollution by generating a significant amount of electrochemical sludge [12]. A 2000 mg/L simulated HPAM wastewater was treated by using Ti/SnO_2-Sb_2O_3 and 304 stainless steel as the anode and cathode, respectively, and a COD removal efficiency of 84% was achieved [13].

Ti/SnO_2-Sb_2O_3 electrodes are easily attacked by oxygen atoms, which causes the exfoliation of the tin antimony active layer and greatly affects the service life of these electrodes. However, they can be used as an intermediate layer to improve the electrode life. PbO_2 is considered a non-active electrode because of its high oxygen overpotential. Ti/PbO_2 electrodes have the advantages of high electrical conductivity, strong oxidizing ability, and low cost, and have been widely used to treat refractory organic pollutant wastewater [14]. It has been reported that hydroxyl radicals exist mainly as adsorbed hydroxyl radicals at the anodes [15]. Contaminants have been found to be completely mineralized on the electrode surface by the direct interaction with adsorbed hydroxyl radicals, as given by Equation (1) [16]:

$$PbO_2(\cdot OH) + \text{organics} \rightarrow PbO_2 + mCO_2 + nH_2O + H^+ + e^- \quad (1)$$

However, pure β-PbO_2 electrode coatings can easily fall off and will dissolve toxic Pb^{2+} [17-19], which in turn will reduce the electrode life. To solve these problems, SnO_2-Sb_2O_3 was prepared as the middle layer between Ti/PbO_2 in the present study. Based on the use of the Ti/SnO_2-Sb_2O_3/β-PbO_2 electrode, the current density, electrode distance, initial pH, and electrolyte concentration of the electrochemical degradation of HPAM were investigated. The HPAM degradation kinetics and mechanism were also studied.

2. METHODOLOGY

2.1 Materials and Reagents

Deionized water (18.2 MΩ·cm) produced by a UPH-I-20T system (ULUPURE, China) was used to prepare all reaction solutions. Oxalic acid ($H_2C_2O_4$), sodium fluoride (NaF), bromine water, hydrofluoric acid (HF), hydrochloric acid (HCl), nitric acid (HNO_3), citric acid ($C_6H_8O_7$), ethylene glycol ($(CH_2OH)_2$), lead nitrate ($Pb(NO_3)_2$), antimony trichloride ($SbCl_3$), stannic chloride ($SnCl_4$), sodium chloride (NaOH), ethylene glycol ($(CH_2OH)_2$), citric acid (CA), sodium formate (HCOONa), soluble starch, anhydrous sodium acetate (CH_3COONa), aluminum sulfate ($Al_2(SO_4)_3$), cadmium iodide (CdI_2), and polyacrylamide (PAM, 3×10^7 DA) were obtained from Chengdu Aikeda Chemical Reagent Co., Ltd. and Beijing Ketuo Chemical Reagent Co., Ltd. (China). All chemicals were of analytical grade.

The simulated HPAM solution was configured by dissolving 200 mg PAM in 1 L deionized water and NaCl. The HPAM model solution initial pH value was 5 ± 0.1.

2.2 Electrode preparation

Titanium plates (99.5%, 30×60×1 mm) were smoothed and polished with 600 P and 1200 P sandpaper, immersed in 40% NaOH solution to degrease them, and then immersed in distilled water for 30 min to obliterate excessive oil on the face. Following, the titanium plates were kept in 20% hydrofluoric acid to remove surface oxides, underwent 10 min of ultrasonic cleaning in deionized water, and were etched in boiling 15% oxalic acid for 2 h and rinsed with deionized water [20].

The SnO_2-Sb_2O_3 coating was fixed on pretreated porous titanium substrates via thermal decomposition. The coating solution consisted of 6.65 g $SnCl_4{\cdot}5H_2O$, 0.475 g $SbCl_3$, 5 ml $CH_2OH)_2$, and 2.5 ml 37% CA. The titanium plates were immersed in this solution for 5 min and then dried in a drying oven at 130 °C for 10 min. This process was repeated ten times. Finally, the plates were transferred to a muffle furnace, calcined for 60 min, and annealed for 120 min [21, 22].

An electrodeposition coating was placed on the outer layer of the β-PbO_2. Electrolysis was conducted at an anodic current density 20 mA/cm^2 for 2 h using the Ti/SnO_2-Sb_2O_3 plate as the cathode. The electrolyte consisted of 260 g/L $Pb(NO_3)$, 65-68% HNO_3, 0.5 g NaF, and 1 mL/L of 47% HF [14].

2.3 Characterization

The surface morphology and composition of the coating were characterized using SEM-EDX (SSX-550, Shimadzu, Japan), and the crystal structures of the coatings and the compositions were scanned using XRD (D8 FOCUS, BRUKER, Germany).

Linear sweep voltammetry (LSV) was employed to characterize the Ti/SnO_2-Sb_2O_3/β-PbO_2 electrode performance, and a standard three-electrode system consisting of the Ti/SnO_2-Sb_2O_3/β-PbO_2 electrode (working electrode), a stainless platinum electrode (counter electrode), and a saturated calomel electrode (SCE) (reference electrode) was measured. A chlorine evolution reaction (CER) was conducted

in a 6 g/L NaCl solution at a scan rate of 10 mV/s. The measurements were carried out with an electrochemical workstation (CHI 660E) controlled by a PC.

2.4 Electrochemical experiment

The experiments in this study were conducted in an 80-mL individual grooved Plexiglas reactor. Ti/SnO_2-Sb_2O_3/β-PbO_2 was used as the anode and stainless steel was used as the cathode. The dimensions of the electrodes were 30×60×1 mm, and 40 mm of the electrodes were immersed in the solution, which was stirred by a magnetic stirrer. The varied operating parameters of the electro-oxidation degradation HPAM experiment were the current density (5-40 mA/cm^2), NaCl concentration (2000-10000 mg/L), electrode distance (1-4 cm), and initial pH (3-11). The initial pH was adjusted using 0.1 mol/L HCl and NaOH.

2.5 Analytical methods

The pH value was measured by a digital pH meter [7]. The HPAM concentration was measured by a starch-iodination method using a UV-vis spectrophotometer analyzer at λ_{max} = 580 nm [23]. The HPAM removal rate was calculated by Equation (2):

$$\text{HPAM removal rate} = C_0 - C_t/C_0 \times 100\% \quad (2)$$

where C_0 (mg/L) is the initial HPAM concentration, and C_t (mg/L) is the final HPAM concentration.

The total organic carbon (TOC) was measured with a Liqui TOC II analyzer (Elementar, Germany) using the combustion-infrared method.

The NO_3^- ion content was detected via ion chromatography (IC) with an ICS-1000 device (Dionex, America). The NH_4-N content was measured by the Nessler reagent photometric method.

The three-dimensional excitation-emission matrix (3D EEM) fluoresce spectra were obtained with a G9800A fluorescence spectrophotometer (Agilent, America). The TOC concentration of the sample was diluted to 5-10 mg/L and subjected to fluorescence scanning after passing through a 0.45-μm pore size acetate membrane. The emission wavelength ranged from 280 to 550 nm, and the initial excitation wavelength was 200 nm. The excitation source was a 150 W xenon lamp with an excitation and emission spectral increment of 10 nm, a scanning speed of 1200 nm/min, and a PMT of 700 V.

The HPAM solid samples for FT-IR were prepared according to the methods provided in the existing literature [24], and the samples were qualitatively analyzed by Fourier transform infrared spectroscopy (FT-IR) (Tensor 27, Bruker, Germany). The FTIR spectra were measured from 4000 cm^{-1} to 400 cm^{-1} with a resolution of 2 cm^{-1}, and the scanned curve was subjected to atmospheric compensation.

The reaction product was analyzed by gas chromatography/mass spectrometry (GC/MS), and the method used for the pretreatment of samples was that described by Lu [25]. GC-MS analysis of samples was carried out using a gas chromatograph system (Agilent, America) equipped with a capillary column (30×0.25 mm, film thickness 0.25 μm). The inlet temperature was 280 °C. The temperature control program was set to start at 40 °C for 2 min and was increased to 290 °C at a rate of 5 °C/min. The injection volume was 1 uL, and the flow rate of He gas was 1.0 mL/min. The electron energy was set at

70 eV. The water sample volume was 80 mL, and the pH of the water samples was adjusted to 2 for the identification of the by-products of the acidic HPAM. The water sample was mixed with 40 mL methane, shaken for 10 min, and left to rest for 15 min. After complete stratification, the organic phase was placed in a 250-mL flask and the water sample was further extracted with 40 mL of dichloromethane. The water sample was repeated three times and dehydrated by adding anhydrous sodium sulfate, filtered, and then placed in a fume hood to evaporate and concentrate to 1 mL. The remaining water was adjusted to a pH of about 12 (alkaline component), and extracted into another flask according to the above method.

2.6 Energy consumption

The energy consumption (kWh/m^3) was calculated by Equation (3):

$$\text{Energy consumption} = \left(\frac{U \times I \times t}{V}\right) \quad (3)$$

where U is the cell voltage (V), I is the electrolysis current (A), t is the reaction time (h), and V is the volume of the sample (m^3).

3. RESULTS AND DISCUSSION

3.1 Characterization of electrodes

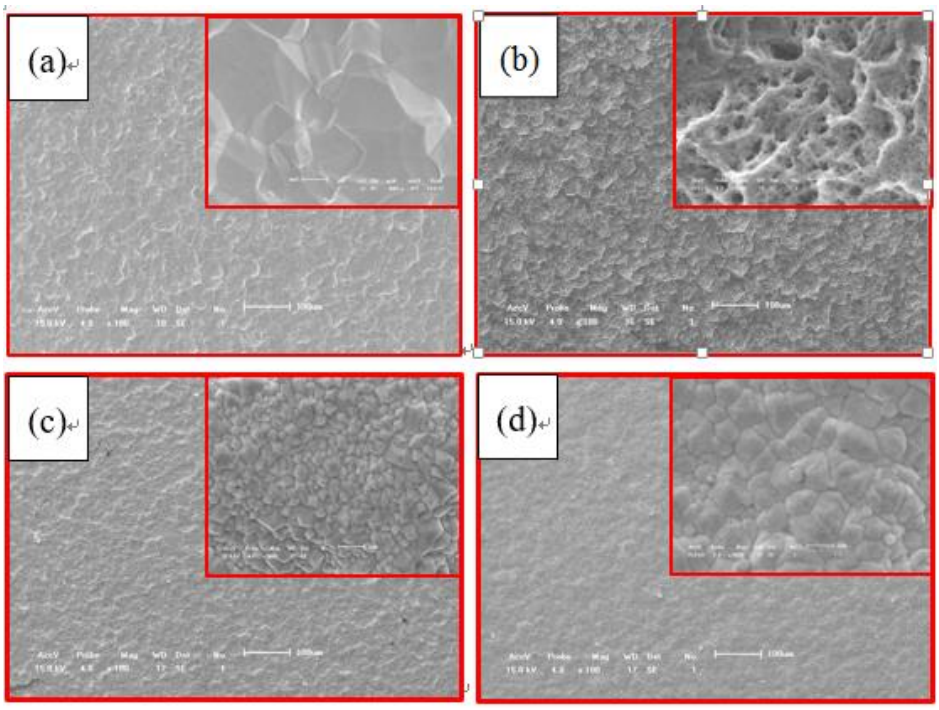

Figure 1. SEM images of different electrodes: (a) Ti; (b) Ti/SnO_2-Sb_2O_3; (c) Ti/β-PbO_2; (d) Ti/SnO_2-Sb_2O_3/β-PbO_2.

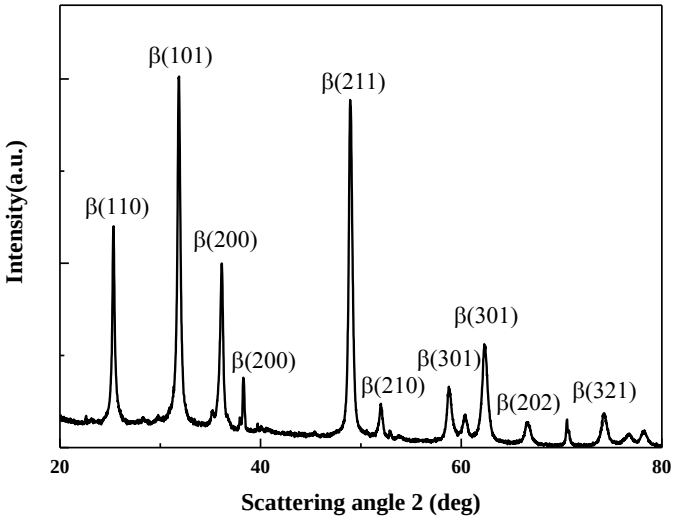

Figure 2. XRD of the Ti/SnO_2-Sb_2O_3/β-PbO_2 electrode.

3.1.1 SEM of different electrodes

Fig. 1 presents the SEM images of different electrodes with average grain sizes of 2 μm and 50 μm, which were used to characterize the morphological structures of the Ti, Ti/SnO_2-Sb_2O_3, Ti/β-PbO_2, and Ti/SnO_2-Sb_2O_3/β-PbO_2 electrodes. Fig. 1(a) depicts the titanium plate after oxalic acid etching, which was characterized by roughness and compactness. This structure has two advantages: first, the titanium substrate has a large surface area, which is conducive to improving its electrochemical properties; second, the rough surface of the titanium substrate can enhance the bonding force between the oxide coating and the titanium substrate, and thus extend the service life of the electrode. The morphology of Ti/SnO_2-Sb_2O_3 is presented in Fig.1(b), from which it can be seen that the coating on the electrode surface was dense and formed a uniform and uneven rocky outer structure, and there was no obvious "crack" phenomenon, indicating that the titanium matrix could be well covered by the coating. Figs. 1(c) and 1(d) respectively exhibit the morphologies of the Ti/β-PbO_2 and Ti/SnO_2-Sb_2O_3/β-PbO_2 electrodes. Compared with the Ti/β-PbO_2 electrode, the surface cracks of the Ti/SnO_2-Sb_2O_3/β-PbO_2 electrode were significantly reduced. This could avoid the diffusion of the new ecological oxygen generated during the electrolysis process to the titanium substrate, alleviate the shedding of the active coating, extend the electrode life, and avoid the generation of TiO_2 with high impedance [22].

3.1.2 XRD of Ti/Sb-Sn_2O_3/β-PbO_2 electrode

Via XRD analysis of the Ti/SnO_2-Sb_2O_3/β-PbO_2 electrode, the phase composition of the PbO_2 deposit can be determined. The result is presented in Fig. 2, in which the diffraction peak of β-PbO_2 is obvious (2θ = (25°, 32°, 36°, 50°, 63°)). The PbO_2 mainly entered the SnO_2 lattice by filling the voids. It was difficult to find the diffraction peaks of Ti and tin antimony oxide, which indicates that the lead dioxide completely covered the electrode [26].

3.2 Linear sweep voltammetry

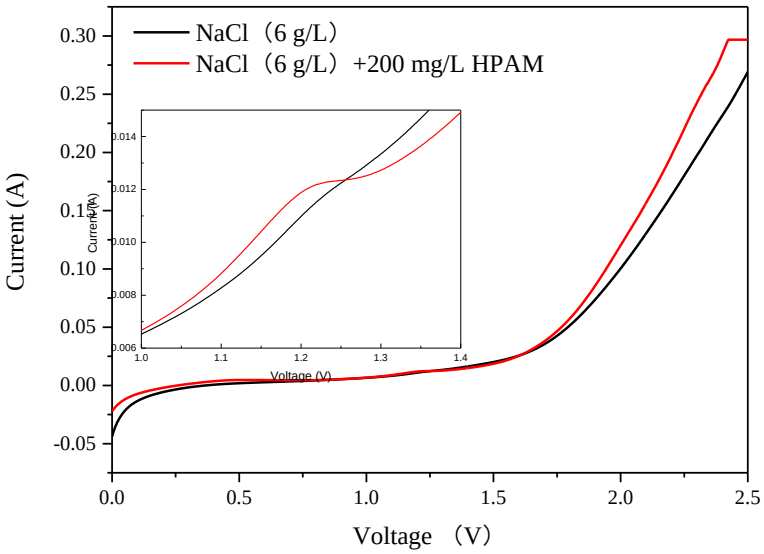

Figure 3. The CER activity of the Ti/SnO_2-Sb_2O_3/β-PbO_2 electrode measured in the solutions of 6 g/L NaCl + 200 mg/L HPAM (red line) and 6 g/L NaCl (black line) as determined by LSV.

Fig. 3 displays the LSV results of the Ti/SnO_2-Sb_2O_3/β-PbO_2 electrode in 0.6 g/L NaCl electrolyte with and without 200 mg/L HPAM. According to the polarization curves, the chlorine evolution potential was approximately 1.5 V (vs. SCE). In the mixed solution, a small peak appeared at 1.2 V (vs. SCE), which is due to the degradation of polyacrylamide. The magnitude of the chlorine evolution potential directly affected the electrochemical performance of the electrode, which had a great influence on the production of reactive chlorine in the reaction system.

3.3 Effect of parameters

3.3.1 Effect of current density

Current density is an important factor in electrochemical processes, and can simultaneously affect work potential and the number of electrons [27]. This is primarily because the reaction system can produce a large number of strong oxidizing substances under a high current density.

In this experiment, the current density was adjusted from 5 to 40 mA/cm^2, and the other operating parameters were as follows: NaCl concentration = 6000 mg/L, electrode distance = 2 cm, and initial pH = 5.

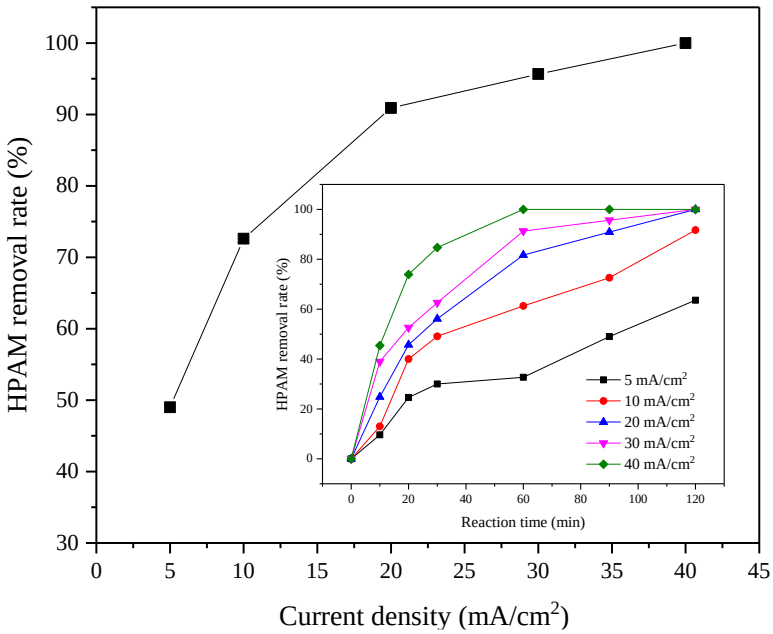

Figure 4. Effect of the current intensity on the removal efficiency of HPAM (conditions: electrode distance 2 cm; initial pH = 5; NaCl concentration = 6000 mg/L; reaction time = 90 min).

As presented in Fig. 4, when the reaction time reached 90 min, the HPAM removal rates were respectively 49%, 72.6%, 90.9%, 95.7%, and 100% by augmenting the current density from 5 to 40 mA/cm^2. The apparent rate constant k_1 and correlation coefficient R^2 are summarized in Table 2. All the correlation coefficients were greater than 0.93, which implies that the electrochemical degradation of HPAM followed pseudo-first-order kinetics. The HPAM removal rate presented an increasing trend with the increase of current density. In the current density range from 5 to 40 mA/cm^2, the k_1 values increased from 7.54×10^{-3} to 49.73×10^{-3} min^{-1}. This is mainly because the increase of current density increased the concentration of hydroxyl radicals and active chlorine, which in turn increased the HPAM removal rate by redox reaction [28, 29]. When the current density exceeded 20 mA/cm^2, the HPAM removal rate did not change significantly due to the intensification of the oxygen evolution reaction (Equation (4)).

$$2H_2O \rightarrow O_2 + 4H^+ + 4e^- \qquad (4)$$

In addition, in the current density range from 20 to 40 mA/cm^2, the energy consumption increased from 9.02 to 26.4 kWh/m^3, thereby indicating that the energy consumption increased significantly when the current density exceeded 20 mA/cm^2. Hence, in the subsequent experiments, a current density of 20 mA/cm^2 was selected as an optimum experimental parameter.

3.3.2 Effect of electrode distance

Electrode distance is also one of the key operating parameters of electrochemical processes, and is very important for energy consumption and pollutant removal efficiency [30]. In this experiment, the electrode distance was adjusted from 1 to 5 cm, and the other operating parameters were as follows: current density = 20 mA/cm^2, NaCl concentration = 6000 mg/L, and initial pH = 5.

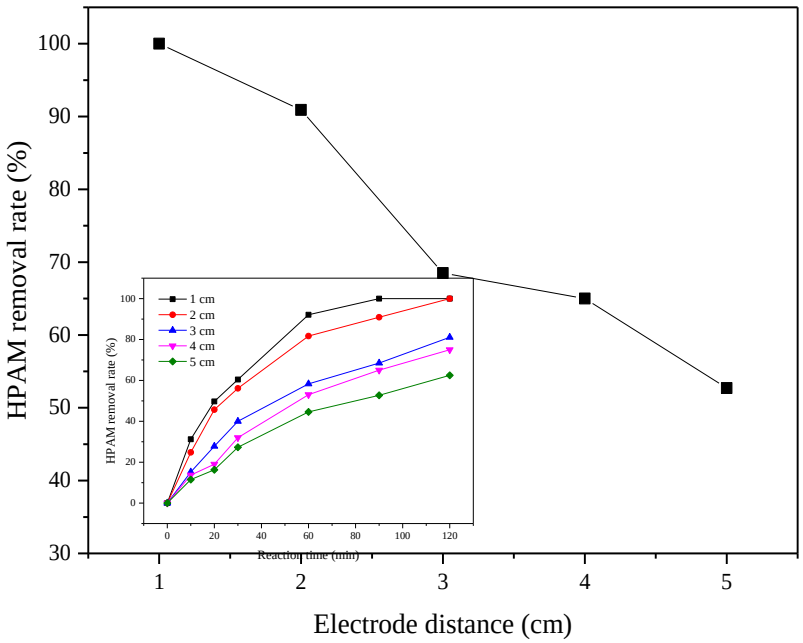

Figure 5. Effect of the electrode distance on the removal of HPAM (conditions: current density = 20 mA/cm^2; initial pH = 5; NaCl concentration = 6000 mg/L; reaction time = 90 min).

As can be seen from Fig. 5, the HPAM removal rate increased as the electrode distance decreased. There was an inverse relationship between the electrode distance and the HPAM removal rate. The results are also presented in Table 2. When the reaction time was 90 min, the HPAM removal rate increased from 52.7% to 100% as the electrode distance decreased from 5 to 1 cm, and the k_1 value increased from 8.07×10^{-3} to 41.89×10^{-3} min^{-1}. This is mainly because the electrode distance determines the magnitude of the electric field strength inside the cell, and the electrode potential was lower at the smaller electrode distance. In addition, a low electrode distance weakens resistance and strengthens the mass transfer efficiency [30]. Moreover, it is worth noting that the energy consumption decreased greatly with the decrease of electrode distance, presenting a decrement from 201.8 to 71.8 kWh/m^3. Therefore, in the subsequent experiments, the electrode distance of 1 cm was selected as an optimum reaction condition.

3.3.3 Effect of initial pH

In general, the initial pH affects the chemical form of active chlorines and the treatment efficiency of pollutants during electrochemical processes. In this experiment, the initial pH was adjusted to 3, 5, 7, 9, and 11. The other operating parameters were as follows: current density = 30 mA, NaCl concentration = 6000 mg/L, and electrode distance = 1 cm.

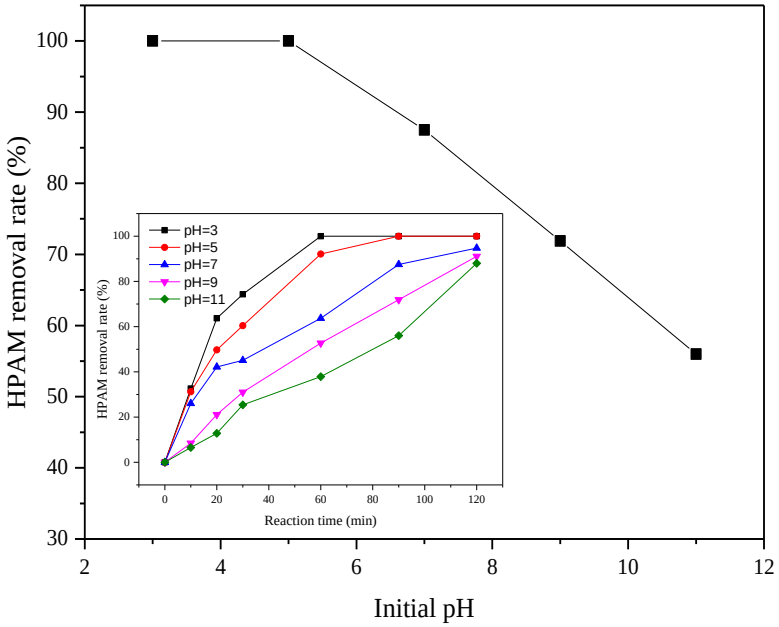

Figure 6. Effect of the initial pH on the removal of HPAM (conditions: current density = 20 mA/cm^2; electrode distance = 1 cm; NaCl concentration = 6000 mg/L; reaction time = 90 min).

As can be seen from Fig. 6, the removal rate of HPAM increased when the pH was decreased from 11.0 to 3.0, which indicates that the removal effect of HPAM under acidic conditions was significantly higher than that under alkaline conditions. As exhibited in Table 2, the reaction rate constant for HPAM removal increased significantly from 9.02×10^{-3} to 46.96×10^{-3} min^{-1} as the initial pH was adjusted from 11 to 3. The pH mainly depends on the influences of active chlorine species (Cl_2/HClO/ClO^-) to influence the electrochemical process [31, 32]. When the initial pH was between 3 and 7, the predominant species were Cl_2 (E^0 = 1.36 V/SHE) and HClO (E^0 = 1.49 V/SHE) (Equations (5) and (6)). In the alkaline solutions of pH > 7, the predominant species was ClO^- (E^0 = 0.89 V/SHE) (Equation (7)) [33]. It is evident that the HPAM was degraded easily in acidic conditions. There was little difference in the removal rates of HPAM at initial pH values of 3 and 5. To reduce the cost of adjusting the pH, the subsequent experiments were performed at an initial pH of 5.

$$Cl^- \rightarrow Cl_{2(aq)} + 2e^- \quad (5)$$

$$Cl_{2(aq)} + H_2O \rightarrow HClO + Cl^- + H^+ \quad (6)$$

$$HClO \rightarrow ClO^- + H^+ \quad (7)$$

3.3.4 Effect of Cl^- concentration

HPAM wastewater usually contains a large amount of chloride ions. The Cl^- concentration has a great influence on the mass transfer efficiency, and is related to the amount of active chlorine produced during the electrochemical process. Therefore, the influence of the electrolyte concentration on the HPAM removal rate was investigated. In this experiment, the NaCl concentration was adjusted from 2000 mg/L to 10000 mg/L, and the other operating parameters were as follows: current density = 20 mA/cm^2, electrode distance = 2 cm, and initial pH = 5.

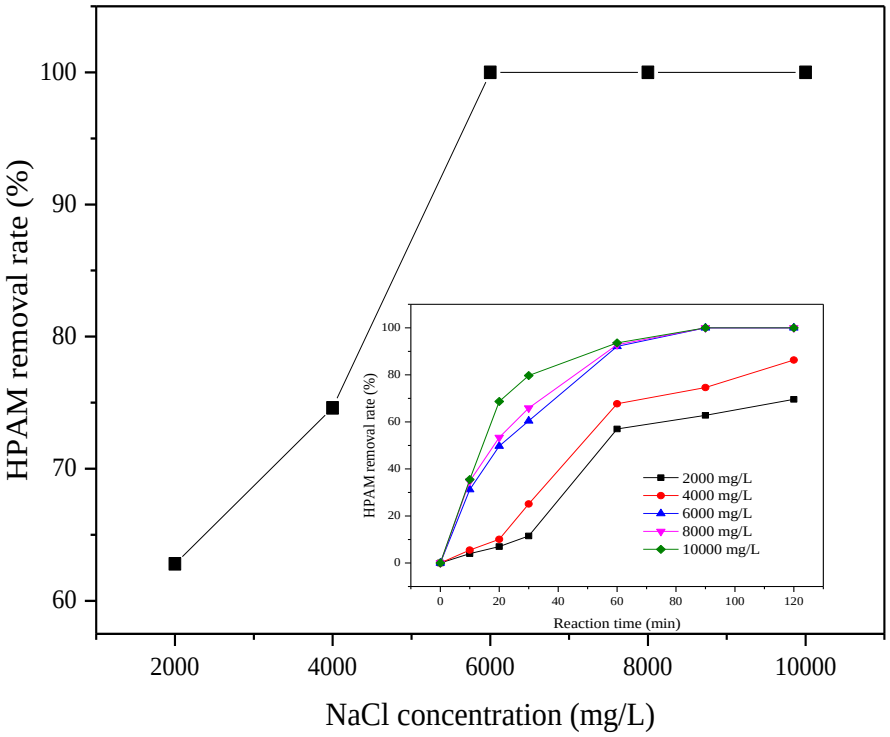

Figure 7. Effect of the current intensity on the removal of HPAM (conditions: current density = 20 mA/cm^2; electrode distance = 1 cm; initial pH = 5; reaction time = 90 min).

The experimental results are presented in Fig. 7, from which it is clear that the HPAM removal efficiency increased with the increase of Cl^- concentration. The HPAM removal rates changed slowly when the chloride ion concentrations were low. During the first 30 min, the HPAM degradation rates were 11.5% and 79.7% at Cl^- concentrations of 2000 mg/L and 10000 mg/L, respectively. This is mainly due to the low content of reactive chlorine that was produced in a low concentration over a short time. It can be observed that when the Cl^- concentration exceeded 6000 mg/L, the HPAM removal rate attained 100% within 90 min; thus, the greater the Cl^- concentration, the more active chlorines were generated. Additionally, under this condition, the applied voltage was lower, which could reduce the power consumption [34]. However, beyond the Cl^- concentration of 6000 mg/L, the HPAM removal rate did not change much. Additionally, the required addition of salt would impose an absolute extra cost and may also result in environmental problems. Accordingly, the optimum concentration of chloride ions was selected as 6000 mg/L.

3.4 Kinetics analysis of HPAM degradation

In this section, the kinetics of all the parameters (current density, electrode distance, initial pH, and electrolyte concentration) during the electrochemical degradation of HPAM are discussed. The zero-order kinetics, first-order kinetics, and second order kinetics of HPAM degradation were respectively determined using the following expressions:

$$A_t - A_0 = -k_0 t \qquad (9)$$

$$\ln\frac{A_t}{A_0} = -k_1 t \quad (10)$$

$$\frac{1}{A_t} = \frac{1}{A_0} + k_2 t \quad (11)$$

where k_0, k_1, and k_2 are respectively the zero-order ($mg \cdot L^{-1} \cdot h^{-1}$), first-order ($min^{-1}$), and second-order ($mg^{-1} \cdot L \cdot h^{-1}$) constants, and *t* is time (min). Table 2 presents the zero-order, first-order, and second-order dynamics constants and regression coefficients obtained using different parameters. The results reveal that the first-order model can better fit the degradation process of HPAM ($R^2 > 0.93$). The maximum reaction rate was 50.57×10^{-3} min^{-1} at a current density of 20 mA/cm^2, electrode distance of 1 cm, initial pH of 5, and electrolyte concentration of 10000 mg/L.

Table 2. Correlation coefficients related to the various tested kinetic models.

Parameters		Zero-order kinetics model		First-order kinetics model		Second-order kinetics model	
		$k_0 \times 10^3$ ($mg \cdot L^{-1} \cdot h^{-1}$)	R^2	$k_1 \times 10^3$ (min^{-1})	R^2	$k_2 \times 10^3$ ($mg^{-1} \cdot L \cdot h^{-1}$)	R^2
Current density (mA/cm^2)	5	424.78	0.92	7.54	0.94	0.13	0.89
	10	1372.73	0.87	18.28	0.93	0.36	0.67
	20	1.469.52	0.88	26.63	0.98	0.52	0.94
	30	1263.64	0.84	34.86	0.98	1.2	0.94
	40	562.03	0.55	49.73	0.97	1.68	0.99
Electrode distance (cm)	5	466.26	0.95	8.07	0.99	0.14	0.99
	4	571.76	0.95	11.66	1.00	0.20	0.98
	3	1118.61	0.93	12.84	0.99	0.21	1.00
	2	1469.52	0.88	35.66	0.98	0.52	0.94
	1	803.52	0.82	41.89	0.97	1.98	0.85
Initial pH	3	1466.43	0.84	46.96	0.98	1.00	1.00
	5	803.52	0.82	41.89	0.97	1.98	0.85
	7	1171.45	0.96	23.48	0.97	0.77	0.69
	9	1382.46	0.99	18.77	0.93	0.41	0.78
	11	822.76	0.97	9.02	0.99	0.12	0.95
Electrolyte concentration ($mg \cdot L^{-1}$)	2000	1452.18	0.87	11.26	0.93	0.10	0.94
	4000	1296.63	0.97	28.57	0.96	1.26	0.56
	6000	803.52	0.82	41.89	0.97	1.98	0.85
	8000	1168.27	0.64	48.76	1.00	0.47	0.79
	10000	2583.75	0.89	50.57	0.98	0.8	0.88

3.5 Degradation pathway of HPAM

3.5.1 TOC, TN, NO_3^- and NH_4^+-N analysis

Under the optimum conditions, simulated wastewater with an HPAM concentration of 200 mg/L was treated to study the variations in TOC, TN, NO_3^-, and NH_4^+-N concentrations during the electrochemical process.

As can be seen from Fig. 8, the TOC and TN concentrations corresponding to 200 mg/L HPAM were 37 mg/L and 15.51 mg/L, respectively; they barely changed within 90 min, and the removal rates

were only 5.82% and 4.32%. This because -NH_2 mainly translates into NO_3^-, nitrogenous organic compounds (NOCs) and ammonia nitrogen (NH_3-N) [35]. When the reaction time was 120 min, the removal rates of TOC and TN were increased to 24.0% and 39.18%, respectively. The concentrations of released NO_3^- and NH_4^+-N were 6.55 mg/L and 0.18 mg/L, respectively. This is mainly because the degradation reaction led to the change of the structures of polyacrylamide side-groups from amide groups to carboxyl groups, and the mineralization of CO_2 and H_2O ultimately led to the reduction of TOC.

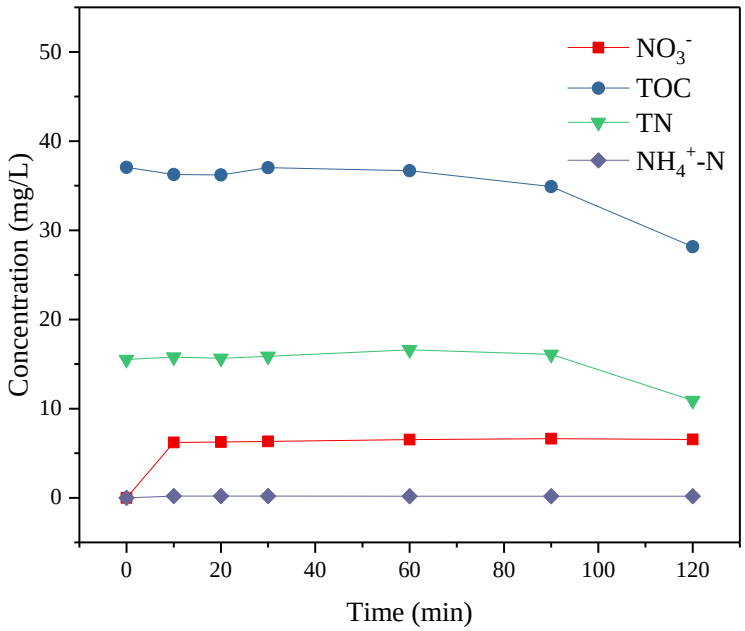

Figure 8. Concentrations of NO_3^-, TOC, TN, and NH_4^+-N at different reaction times (conditions: current density = 20 mA/cm^2; electrode distance = 1 cm; initial pH = 5; NaCl concentration = 6000 mg/L).

3.5.2 Three-dimensional fluorescence spectra

To investigate the degradation pathways of HPAM, three-dimensional excitation emission matrix (3D EEM) fluorescence spectra were analyzed to characterize organic compounds with different fluorescence peaks.

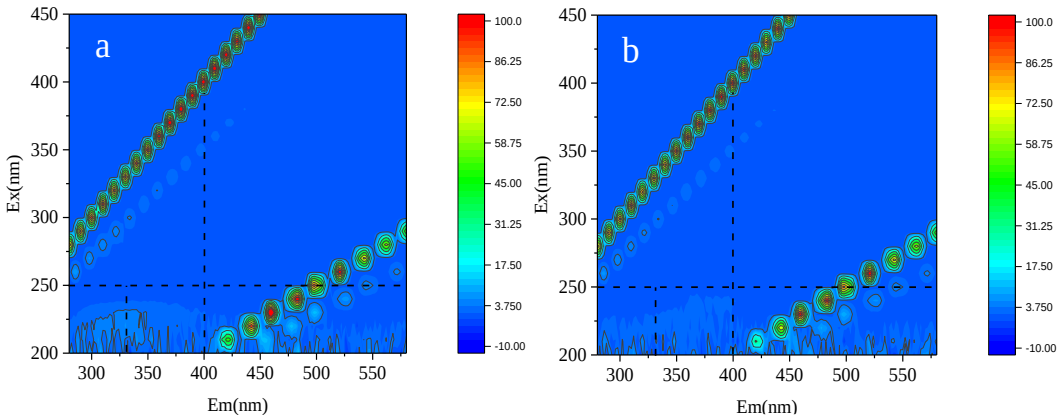

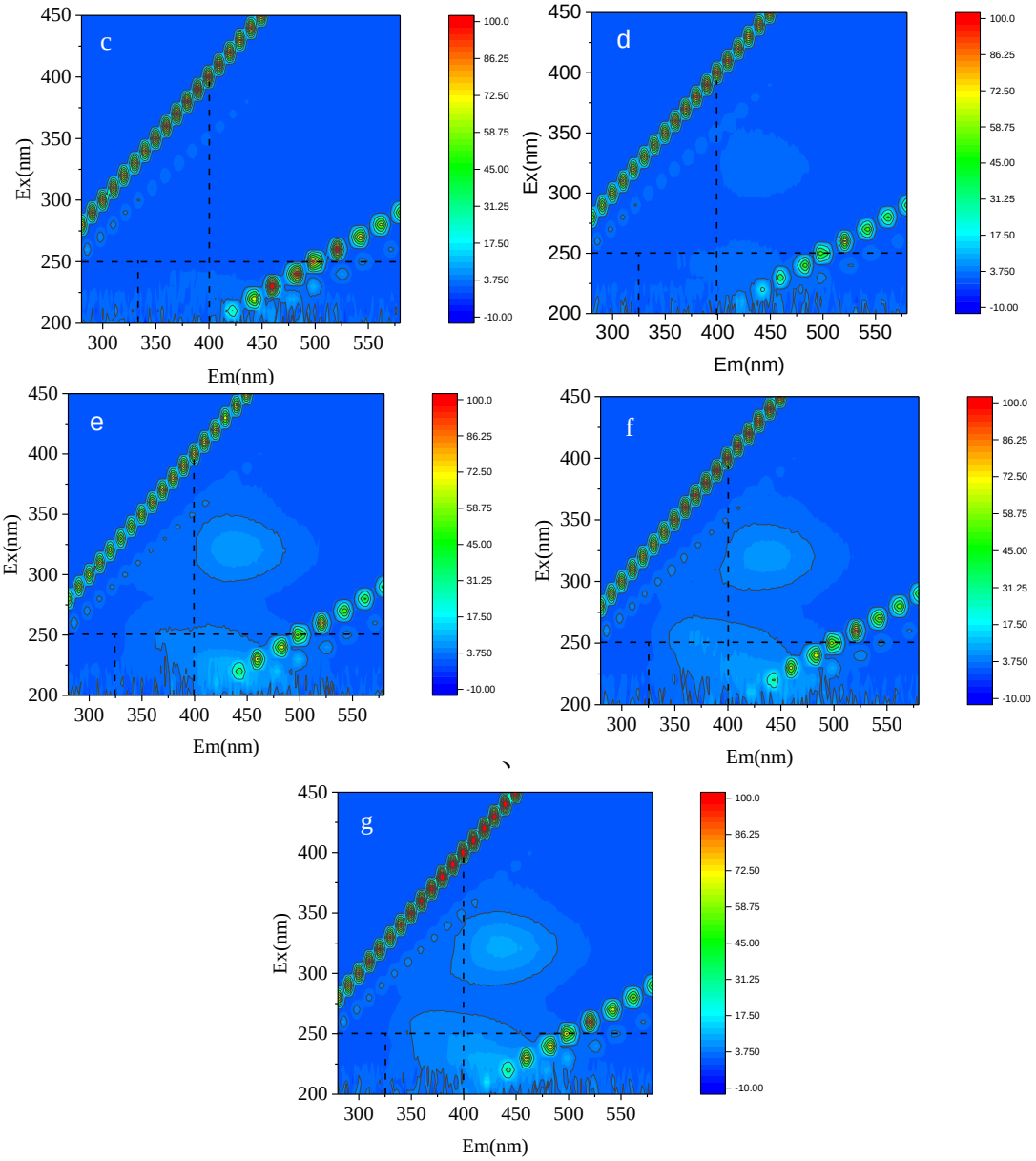

Figure 9. 3D EEM spectra of HPAM solutions at different reaction times (conditions: current density = 20 mA/cm^2; electrode distance = 1 cm; initial pH = 5; NaCl concentration = 6000 mg/L; reaction time = (a) 0 min, (b) 10 min, (c) 20 min, (d) 30 min, (e) 60 min, (f) 90 min, (g) 120 min).

3D EEM spectra can be used to characterize organic compounds with different fluorescence peaks. EEM spectra are usually divided into five regions corresponding to the five groups of different organic compounds, namely aromatic protein I (I, Ex 220-250 nm, Em 280-330 nm), aromatic protein II (II, Ex 220-250 nm, Em 330-380 nm), fulvic acid-like (III, Ex 220-250 nm, Em 380-450 nm), soluble microbial by-product-like (IV, Ex 250-400 nm, Em 280-380 nm), and humic acid-like (V, Ex 250-400 nm, Em 380-500 nm) [36]. As shown in Fig. 9, without any treatment to the HPAM solution, the peak of the fluorescence spectra was identified at the excitation/emission wavelengths (Ex/Em) of 200-250/280-400 nm. Fig. 9b shows that the density of the peak at 200-250/280-400 nm was reduced, which indicates that the HPAM concentration decreased. As the reaction time increased, the fluorescence transferred to regions III and IV. This result indicates that the main degradation products of HPAM were fulvic acid-like and humic acid-like at the reaction time of 30 min. After that, the densities of the peaks

at regions III and IV gradually deepened and moved to region V. Therefore, 3D EEMs analysis confirmed the pollutant transformation in the electro-oxidation reaction of HPAM.

3.5.3 FT-IR analysis

To study the changes in the molecular structure of HPAM, the FT-IR spectra of different HPAM samples were analyzed. Fig. 10 presents the infrared spectra of the HPAM solution before and after electrochemical degradation.

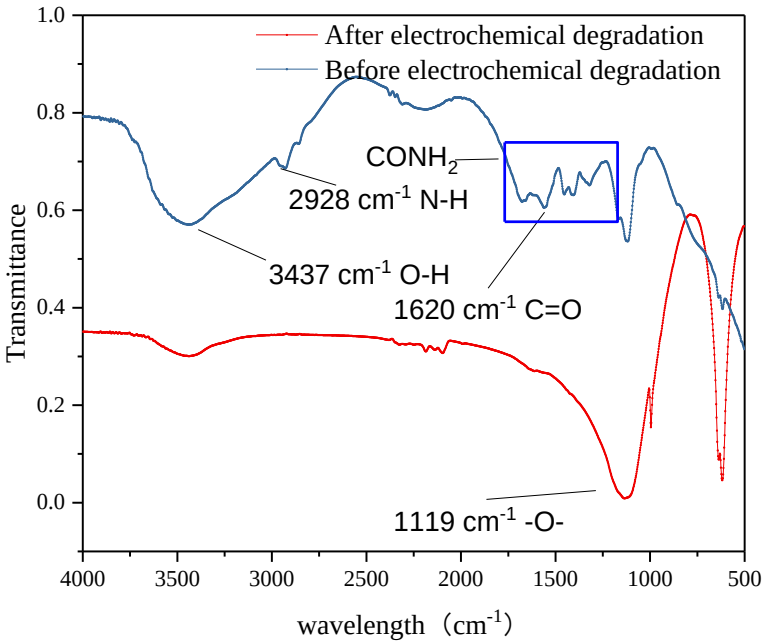

Figure 10. FT-IR analysis of different HPAM samples before and after reaction (conditions: current density = 20 mA/cm^2; electrode distance = 1 cm; initial pH = 5; NaCl concentration = 6000 mg/L; reaction time = 90 min).

The blue line represents the infrared curve before HPAM degradation, and the functional peaks of HPAM are evident. The bands at 3437 cm^{-1} and 2928 cm^{-1} may represent the characteristic absorption peaks of -OH, -NH_2, and methylene (-CH_2). The band at 1620 cm^{-1} could be assigned to the -C=O. characteristic peaks, such as those at 1676 cm^{-1}, 1658 cm^{-1}, 1620 cm^{-1}, 1610 cm^{-1} 1560 cm^{-1}, and 1456 cm^{-1}, which represent amide groups (-$CONH_2$) [35]. The red line represents the infrared curve of the product after electrochemical degradation. It can be seen that a series of characteristic peaks representing -$CONH_2$ disappeared, indicating that the -$CONH_2$ in the polyacrylamide had been degraded by electrooxidation. In addition, an ether group (-O-) appeared at 1119 cm^{-1}, indicating that an ether substance was produced under electrooxidation.

3.5.4 GC/MC analysis.

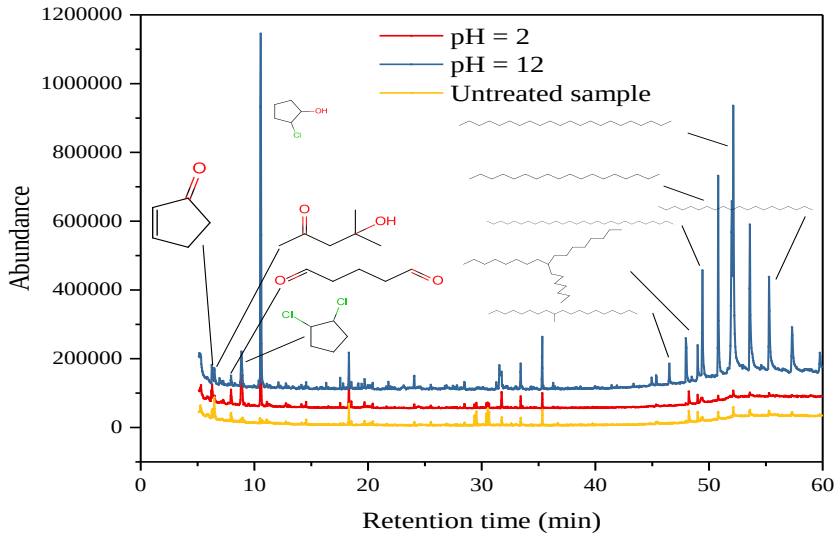

Figure 11. GC-MS of HPAM sample before and after electrochemical treatment (conditions: current density = 20 mA/cm^2; electrode distance = 1 cm; initial pH = 5; NaCl concentration = 6000 mg/L; reaction time = 90 min).

The yellow line, red line, and blue line in Fig. 11 correspond to extraction under untreated, acidic, and alkaline conditions, respectively. There were many ion current peaks after electrochemical treatment, which indicates that HPAM occurred during aeration. The backbone of HPAM was broken, thus producing a large number of low-mass oligomers that may have been oligomeric derivatives of HPAM containing double bonds. The fracture of carbon chains and amine groups occurred under the attack of ·OH and hypochlorous acid, which produced small-molecule alkane, epoxy, and carbonyl groups.

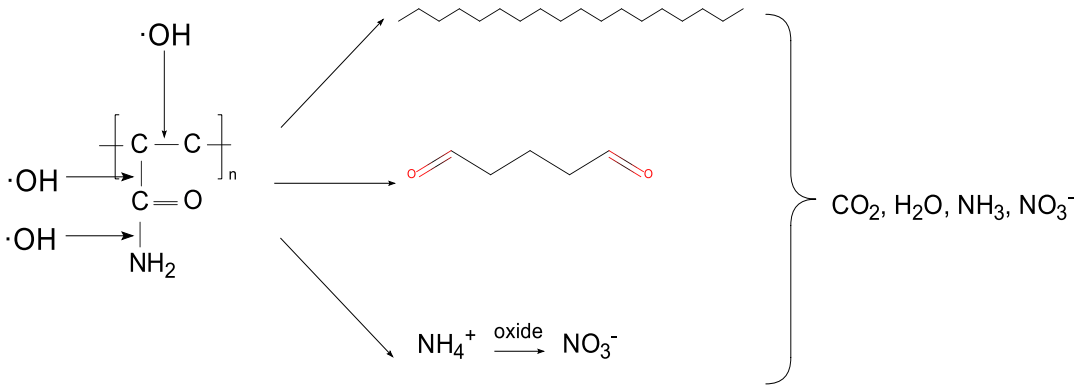

Figure 12. Hypothetical degradation pathways of HPAM during electrochemical treatment.

In consideration of the preceding analysis, the degradation pathway of HPAM via electrochemical treatment is proposed, as presented in Fig. 12. Under the attack of a strong oxidant, the main chain of carbon is broken to form alkanes, the side chain of carbon is broken to form carbonyl

oxide, and the amide group is oxidized to NH_4^+ and NO_3^-. Finally, these small molecules are partially oxidized into CO_2 and H_2O, which is consistent with the decrease of TOC. The decrease of total nitrogen is mainly related to the production of free ammonia (NH_3).

4. CONCLUSION

In this study, Ti/SnO_2+Sb_2O_3/β-PbO_2 and stainless steel were respectively used as anodes and cathodes to produce a high HPAM degradation rate. The electrocatalytic degradation of HPAM wastewater was found to conform to the kinetics of apparent first-order reaction. The maximum reaction rate was 50.57×10^{-3} min^{-1} at a current density of 20 mA/cm^2, electrode distance of 1 cm, initial pH of 5, and Cl^- concentration of 10000 mg/L. The HPAM, TOC, and TN removal rates were 100%, 24.0%, and 39.18%, respectively. The degradation products of HPAM were analyzed via 3D EEM, IC, FT-IR, and GC-MS, and the degradation mechanism was discussed. It was speculated that the degradation of HPAM mainly included the conversion of the carbon main chains into small carbon chains, the conversion of amide groups into NH_4^+ and nitrate NO_3^-, and the formation of ether bonds through intermolecular condensation.

ACKNOWLEDGEMENT

This work was supported by the National Natural Science Foundation of China (Grant No. 21677018), the Joint Fund of the Beijing Natural Science Foundation and Beijing Municipal Education Commission (Grant No. KZ201810017024), and the Open Project Program of the State Key Laboratory of Petroleum Pollution Control (Grant No. PPC2017006), CNPC Research Institute of Safety and Environmental Technology.

References

1. X. Shen, L. Lu, B.Y. Gao, X. Xu and Q.Y. Yue, *Front. Environ. Sci. Eng. China.*, 13 (2019) 1.
2. L. Zhang, F. Su, N. Wang, S. Liu, M. Yang, Y.Z. Wang, D. Huo and T. Zhao, *Bioresour. Technol.*, 278 (2019) 99.
3. J. Xu, C. Ma, B.Q. Cao, J. Bao, Y. Sun, W.X. Shi and S.L. Yu, *Process Saf. Environ. Prot.*, 103 (2016) 564.
4. X.Y. Zhang, S.S. Gao, J.Y. Tian, S.J. Shan, R. Takagi, F.Y. Cui, L.M. Bai and H. Matsuyama, *Ind. Eng. Chem. Res.*, 58 (2019) 994.
5. B.Y. Gao, Y.Y. Jia, Y.Q. Zhang, Q.A. Li and Q.Y. Yue, *J. Environ. Sci.*, 23 (2011) 37.
6. M. Duan, Y.Z. Ma, S.W. Fang, P. Shi, J. Zhang and B. Jing, *Sep. Purif. Technol.*, 133 (2014) 160.
7. Y.R. Pi, Z.H. Zheng, M.T. Bao, Y. Li, Y. Zhou and G. Sang, *Chem. Eng. J.*, 273 (2015) 1.
8. L. Zhao, M. Bao, M. Yan and J. Lu, *Bioresour. Technol.*, 216 (2016) 95.
9. I.C. Eleoterio, J.C. Forti and A.R. de Andrade, *Electroanalysis*, 4 (2013) 283.
10. P. Kaur, J.P. Kushwaha and V.K. Sangal, *Process Saf. Environ. Prot.*, 111 (2017) 13.
11. W.C. Cho, K.M. Poo, H.O. Mohamed, T.N. Kim, Y.S. Kim, M.H. Hwang, D.W. Jung and K.J. Chae, *Chemosphere*, 206 (2018) 483.
12. M.J. Zhu, J. Yao, W.B. Wang, X.Q. Yin, W. Chen and X.Y. Wu, *Desalin. Water. Treat.*, 57 (2016) 15314.
13. Z.H. Kang, H.K. Li, Y.H. Xu and L. Chen, *Desalin. Water. Treat.*, 51 (2013) 2687.

14. Y. Zheng, W. Su, S. Chen, X. Wu and X. Chen, *Chem. Eng. J.*, 174 (2011) 304.
15. S. Song, L. Zhan, Z. He, L. Lin, J. Tu, Z. Zhang, J. Chen and L. Xu, *J. Hazard. Mater.*, 175 (2010) 614.
16. S. Song, J. Fan, Z. He, L. Zhan, Z. Liu, J. Chen and X. Xu, *Electrochim. Acta*, 55 (2010) 3606.
17. J. Zhao, C. Zhu, J. Lu, C. Hu, S. Peng and T. Chen, *Electrochim. Acta*, 118 (2014) 169.
18. Z. He, M.D. Hayat, X.W. Yuan, X. Wang and P. Cao, *J. Appl. Electrochem.*, 48 (2018) 783.
19. X.L. Li, H. Xu and W. Yan, *J. Alloys. Compd.*, 718 (2017) 386.
20. Q.L. Zhang, X.Y. Guo, X.D. Cao, D. Wang and J. Wei, *Chin. J. Catal.*, 36 (2015) 975.
21. J. Xing, D. Chen, W. Zhao, X. Peng, Z. Bai, W. Zhang and X. Zhao, *RSC Adv.*, 5 (2015) 53504.
22. H. An, Q. Li, D. Tao, H. Cui, X. Xu, L. Ding, L. Sun and J. Zhai, *Appl. Surf. Sci.*, 258 (2011) 218.
23. G. Sang, Y. Pi, M. Bao, Y. Li and J. Lu, *Ecol. Eng.*, 84 (2015) 121.
24. M. Bao, Q. Chen, Y. Li and G. Jiang, *J. Hazard. Mater.*, 184 (2010) 105.
25. M. Lu, X. Wei, *Bioresour. Technol.*, 102 (2011) 2555.
26. X. Li, H. Xu, W. Yan and D. Shao, *J. Electroanal. Chem.*, 775 (2016) 43.
27. S.Q. Yang, Y.H. Cui, Y.Y. Liu, Z.Q. Liu and X.Y. Li, *Sep. Purif. Technol.*, 207 (2018) 461.
28. G.R.D. Oliveira, N.S. Fernandes, J.V.D. Melo, D.R.D. Silva, C. Urgeghe and C.A. MartiNez-Huitle, *Chem. Eng. J.*, 168 (2011) 208.
29. M. Yoosefian, S. Ahmadzadeh, M. Aghasi and M. Dolatabadi, *J. Mol. Liq.*, 225 (2017) 544.
30. L. Xu, G. Cao, X. Xu, C. He, Y. Wang, Q. Huang and M. Yang, *Sep. Purif. Technol.*, 195 (2018) 121.
31. M.G. Tavares, L.V.A. da Silva, A.M. Sales Solano, J. Tonholo, C.A. Martinez-Huitle and C.L.P.S. Zanta, *Chem. Eng. J.*, 204 (2012) 141.
32. D.G. Bassyouni, H.A. Hamad, E.S.Z. El-Ashtoukhy, N.K. Amin and M.M. Abd El-Latif, *J. Hazard. Mater.*, 335 (2017) 178.
33. C. Bruguera-Casamada, I. Sires, E. Brillas and R.M. Araujo, *Sep. Purif. Technol.*, 178 (2017) 224.
34. Q.Z. Dai, J.Z. Zhou, X.Y. Meng, D. Feng, C. Wu and J. Chen, *Chem. Eng. J.*, 289 (2016) 239.
35. W. Song, Y. Zhang, J. Yu, Y. Gao, T. Naitoc, G. Oinumac, Y. Inanagac and M. Yang, *J. Environ. Sci.*, 83 (2019) 1.
36. D. Wu, C. Zhou, G. Lu, Y. Zhou and Y. Shen, *Sep. Purif. Technol.*, 227 (2019) 115715.